American Mineralogist, Volume 95, pages 1560–1568, 2010

Lead-tellurium oxysalts from Otto Mountain near Baker, California: V. Timroseite, $Pb_2Cu_5^{2+}(Te^{6+}O_6)_2(OH)_2$, and paratimroseite, $Pb_2Cu_4^{2+}(Te^{6+}O_6)_2(H_2O)_2$, two new tellurates with Te-Cu polyhedral sheets

ANTHONY R. KAMPF,[1,]* STUART J. MILLS,[2] ROBERT M. HOUSLEY,[3] JOSEPH MARTY,[4] AND BRENT THORNE[5]

[1]Mineral Sciences Department, Natural History Museum of Los Angeles County, 900 Exposition Blvd., Los Angeles, California 90007, U.S.A.
[2]Department of Earth and Ocean Sciences, University of British Columbia, Vancouver, British Columbia V6T 1Z4, Canada
[3]Division of Geological and Planetary Sciences, California Institute of Technology, Pasadena, California 91125, U.S.A.
[4]3457 E. Silver Oak Road, Salt Lake City, Utah 84108, U.S.A.
[5]3898 S. Newport Circle, Bountiful, Utah 84010, U.S.A.

ABSTRACT

Timroseite, $Pb_2Cu_5^{2+}(Te^{6+}O_6)_2(OH)_2$, and paratimroseite, $Pb_2Cu_4^{2+}(Te^{6+}O_6)_2(H_2O)_2$, are two new tellurates from Otto Mountain near Baker, California. Timroseite is named in honor of Timothy (Tim) P. Rose and paratimroseite is named for its relationship to timroseite. Both new minerals occur on fracture surfaces and in small vugs in brecciated quartz veins. Timroseite is directly associated with acanthite, cerussite, bromine-rich chlorargyrite, chrysocolla, gold, housleyite, iodargyrite, khinite-4*O*, markcooperite, ottoite, paratimroseite, thorneite, vauquelinite, and wulfenite. Paratimroseite is directly associated with calcite, cerussite, housleyite, khinite-4*O*, markcooperite, and timroseite. Timroseite is orthorhombic, space group $P2_1nm$, a = 5.2000(2), b = 9.6225(4), c = 11.5340(5) Å, V = 577.13(4) Å^3, and Z = 2. Paratimroseite is orthorhombic, space group $P2_12_12_1$, a = 5.1943(4), b = 9.6198(10), c = 11.6746(11) Å, V = 583.35(9) Å^3, and Z = 2. Timroseite commonly occurs as olive to lime green, irregular, rounded masses and rarely in crystals as dark olive green, equant rhombs, and diamond-shaped plates in subparallel sheaf-like aggregates. It has a very pale yellowish green streak, dull to adamantine luster, a hardness of about 2½ (Mohs), brittle tenacity, irregular fracture, no cleavage, and a calculated density of 6.981 g/cm^3. Paratimroseite occurs as vibrant "neon" green blades typically intergrown in irregular clusters and as lime green botryoids. It has a very pale green streak, dull to adamantine luster, a hardness of about 3 (Mohs), brittle tenacity, irregular fracture, good {001} cleavage, and a calculated density of 6.556 g/cm^3. Timroseite is biaxial (+) with a large 2V, indices of refraction > 2, orientation X = **b**, Y = **a**, Z = **c** and pleochroism: X = greenish yellow, Y = yellowish green, Z = dark green ($Z > Y > X$). Paratimroseite is biaxial (–) with a large 2V, indices of refraction > 2, orientation X = **c**, Y = **b**, Z = **a** and pleochroism: X = light green, Y = green, Z = green ($Y = Z >> X$). Electron microprobe analysis of timroseite provided PbO 35.85, CuO 29.57, TeO_3 27.75, Cl 0.04, H_2O 1.38 (structure), O≡Cl –0.01, total 94.58 wt%; the empirical formula (based on O+Cl = 14) is $Pb_{2.07}Cu_{4.80}^{2+}Te_{2.04}^{6+}O_{12}(OH)_{1.98}Cl_{0.02}$. Electron microprobe analysis of paratimroseite provided PbO 36.11, CuO 26.27, TeO_3 29.80, Cl 0.04, H_2O 3.01 (structure), O≡Cl –0.01, total 95.22 wt%; the empirical formula (based on O+Cl = 14) is $Pb_{1.94}Cu_{3.96}^{2+}Te_{2.03}^{6+}O_{12}(H_2O)_{1.99}Cl_{0.01}$. The strongest powder X-ray diffraction lines for timroseite are [d_{obs} in Å (*hkl*) *I*]: 3.693 (022) 43, 3.578 (112) 44, 3.008 (023) 84, 2.950 (113) 88, 2.732 (130) 100, 1.785 (multiple) 33, 1.475 (332) 36; and for paratimroseite 4.771 (101) 76, 4.463 (021) 32, 3.544 (120) 44, 3.029 (023,122) 100, 2.973 (113) 48, 2.665 (131) 41, 2.469 (114) 40, 2.246 (221) 34. The crystal structures of timroseite (R_1 = 0.029) and paratimroseite (R_1 = 0.039) are very closely related. The structures are based upon edge- and corner-sharing sheets of Te and Cu polyhedra parallel to (001) and the sheets in both structures are identical in topology and virtually identical in geometry. In timroseite, the sheets are joined to one another along c by sharing the apical O atoms of Cu octahedra, as well as by sharing edges and corners with an additional CuO_5 square pyramid located between the sheets. The sheets in paratimroseite are joined only via Pb-O and H bonds.

Keywords: Timroseite, paratimroseite, new mineral, tellurate, crystal structure, Otto Mountain, California

INTRODUCTION

Timroseite, $Pb_2Cu_5^{2+}(Te^{6+}O_6)_2(OH)_2$, and paratimroseite, $Pb_2Cu_4^{2+}(Te^{6+}O_6)_2(H_2O)_2$, are among seven new secondary lead-tellurium minerals discovered recently at Otto Mountain near Baker, California. Detailed information on the mining history, geology, mineralogy, and mineral paragenesis of the deposit, as well as on the discovery of the new minerals, is provided in Kampf et al. (2010b).

Timroseite is named in honor of Timothy (Tim) P. Rose (b. 1960) and paratimroseite is named for its relationship to tim-

* E-mail: akampf@nhm.org

roseite. Rose is a geochemist at Lawrence Livermore National Laboratory and an avid mineral collector. He collected and provided two of the three cotype specimens of timroseite for study, from which the only crystals suitable for single-crystal work were obtained. Rose has agreed to the naming of timroseite in his honor. The new minerals and names have been approved by the Commission on New Minerals, Nomenclature and Classification of the International Mineralogical Association (timroseite: IMA 2009-064 and paratimroseite: IMA 2009-065). Three cotype specimens of timroseite (catalog numbers 62531, 62532, and 62533) and two of paratimroseite (catalog numbers 62263 and 62534) are deposited in the Natural History Museum of Los Angeles County.

OCCURRENCE

Timroseite was found at the Aga mine, (35° 16.399′N 116° 05.665′W) on Otto Mountain, ~2 km northwest of Baker, San Bernardino County, California, U.S.A., and in the Bird Nest drift on the southwest flank of Otto Mountain, 0.7 km northwest of the Aga mine (35° 16.606′N 116° 05.956′W). Paratimroseite is considerably rarer and is known only from a few specimens from at the Aga mine. We have also confirmed timroseite as occurring as lime green botryoids at the Vesley mine, Granite Gap, Hidalgo County, New Mexico.

Both minerals occur on fracture surfaces and in small vugs in quartz veins. Timroseite is directly associated with acanthite, cerussite, bromine-rich chlorargyrite, chrysocolla, gold, iodargyrite, khinite-4*O*, vauquelinite, wulfenite, and the new minerals housleyite [$Pb_6Cu^{2+}Te^{6+}_4O_{18}(OH)_2$] [IMA2009-024; Kampf et al. (2010c)], markcooperite [$Pb_2(UO_2)Te^{6+}O_6$] [IMA2009-045; Kampf et al. (2010d)], ottoite [$Pb_2Te^{6+}O_5$] [IMA2009-063; Kampf et al. (2010b)], paratimroseite and thorneite [$Pb_6(Te^{6+}_2O_{10})(CO_3)Cl_2(H_2O)$] [IMA2009-023; Kampf et al. (2010a)]. Paratimroseite is directly associated with calcite, cerussite, housleyite, khinite-4*O*, markcooperite and timroseite. Note that powder X-ray diffraction of khinite crystals on paratimroseite cotype specimen 62534 showed them to probably be a combination of the khinite-4*O* and khinite-3*T* polytypes. This was the only evidence of the khinite-3*T* polytype on any specimen from Otto Mountain examined. Other species identified in the Otto Mountain assemblages include: anglesite, atacamite, boleite, brochantite, burckhardtite, caledonite, celestine, chalcopyrite, devilline, diaboleite, fluorite, fornacite, galena, goethite, jarosite, kuranakhite, linarite, malachite, mimetite, mottramite, munakataite, murdochite, muscovite, perite, phosphohedyphane, plumbojarosite, pyrite, schieffelinite, vanadinite, and one other new mineral: telluroperite [$Pb_3Te^{4+}O_4Cl_2$] [IMA2009-044; Kampf et al. (2010e)]. Other potentially new species are still under investigation.

Timroseite and paratimroseite and most the other secondary minerals of the quartz veins are interpreted as having formed from the partial oxidation of primary sulfides (e.g., galena and chalcopyrite) and tellurides (e.g., hessite) during or following brecciation of the quartz veins.

PHYSICAL AND OPTICAL PROPERTIES

Timroseite

Timroseite most commonly occurs as olive to lime green irregular rounded crystalline masses (Fig. 1) and very rarely as distinct crystals in the form of dark olive green equant rhombs or diamond-shaped plates in subparallel sheaf-like aggregates to 0.5 mm. Crystals exhibit the forms {001}, {110}, and {010} (Fig. 2). No twinning was observed. The mineral is non-fluorescent. The streak is a very pale yellowish green and the luster is dull to adamantine. The Mohs hardness is estimated at 2½. The mineral is brittle with irregular fracture and has no cleavage. The density could not be measured because it is greater than those of available high-density liquids and there is insufficient material for physical measurement. The calculated density for the ideal formula is 6.982 g/cm³. In dilute HCl, timroseite immediately decomposes, turning opaque white, and then the residue slowly dissolves.

FIGURE 1. SEM image of timroseite showing the surface of an irregular rounded crystalline mass.

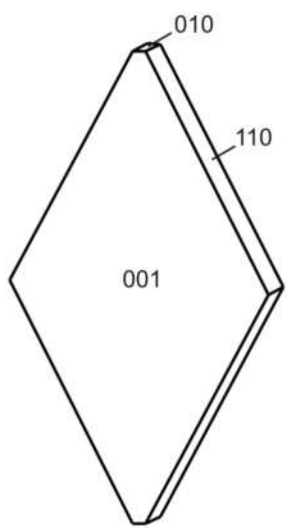

FIGURE 2. Crystal drawing of timroseite (clinographic projection).

The indices of refraction exceed those of available index fluids. The Gladstone-Dale relationship (Mandarino 1981) predicts n_{av} = 2.113 based on the ideal formula. Orthoscopic and conoscopic optical examination using a Leitz Ortholux I polarizing microscope equipped with a Supper spindle stage showed timroseite to be biaxial (+) with a large 2*V*. No dispersion was observed. The optical orientation is *X* = **b**, *Y* = **a**, *Z* = **c** and the pleochroism is *X* = greenish yellow, *Y* = yellowish green, and *Z* = dark green (*Z* > *Y* > *X*).

Paratimroseite

Paratimroseite occurs as vibrant "neon" green blades up to about 0.1 mm in length. Blades typically are intergrown in irregular clusters (Fig. 3). The mineral also occurs in lime green botryoids up to 0.2 mm in diameter. Blades are elongated on [100], flattened on {001}, and exhibit the forms {001}, {010}, {120}, and {100} (Fig. 4). No twinning was observed. The mineral is non-fluorescent. The streak is a very pale green, and the luster is adamantine for crystals and dull for botryoids. The Mohs hardness is estimated at 3. The mineral is brittle with irregular fracture and good {001} cleavage. As for timroseite, density could not be measured. The calculated density for the ideal formula is 6.557 g/cm^3. In dilute HCl paratimroseite also immediately decomposes, turning opaque white, and then the residue slowly dissolves.

The indices of refraction exceed those of available index fluids. The Gladstone-Dale relationship (Mandarino 1981) predicts n_{av} = 2.059 based on the ideal formula. Paratimroseite is biaxial (–) with a large 2*V*. No dispersion was observed. The optical orientation is *X* = **c**, *Y* = **b**, *Z* = **a** and the pleochroism is *X* = light green, *Y* = green, and *Z* = green (*Y* = *Z* >> *X*).

CHEMISTRY

Chemical analyses were carried out using a JEOL8200 electron microprobe (WDS mode, 15 kV, 10 nA, 5 μm beam diameter) at the Division of Geological and Planetary Sciences, California Institute of Technology. The standards used were: PbS, Cu metal, Te metal, and sodalite (for Cl). Five analyses were obtained for both timroseite and paratimroseite. The crystals of both species are quite prone to electron beam damage. This and sample porosity contributes to the low analytical totals, even though we used the mildest analytical conditions feasible. This problem of sample instability in the electron beam appears to be common in tellurates (cf. Grundler et al. 2008; Mills et al. 2008, 2009b, 2010). The material available was insufficient for direct H_2O determination, so it was calculated by stoichiometry from the results of the crystal-structure analysis.

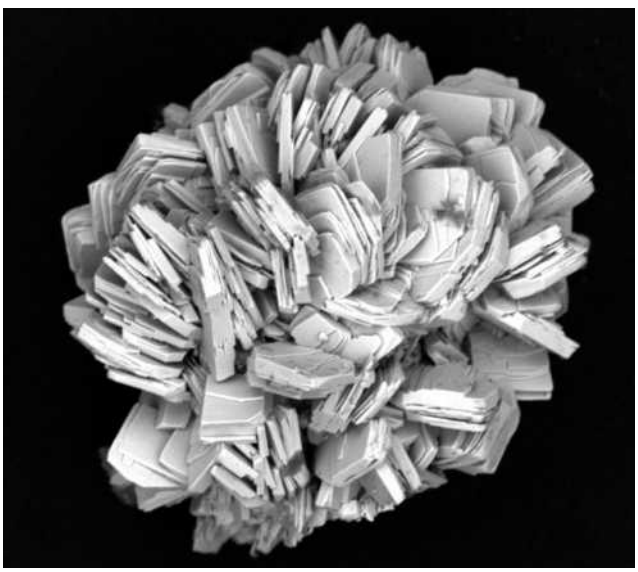

FIGURE 3. SEM image of paratimroseite (FOV 0.15 mm).

Timroseite

The averages (and ranges) of the analyses are: PbO 35.85 (35.51–36.22), CuO 29.57 (29.18–30.02), TeO_3 27.75 (27.36–28.21), Cl 0.04 (0.02–0.06), H_2O 1.38 (structure), O≡Cl –0.01, total 94.58 wt%. The empirical formula (based on O+Cl = 14) is $Pb_{2.07}Cu^{2+}_{4.80}Te^{6+}_{2.04}O_{12}(OH)_{1.98}Cl_{0.02}$. The simplified formula is $Pb_2Cu^{2+}_5(Te^{6+}O_6)_2(OH)_2$, which requires PbO 36.79, CuO 32.78, TeO_3 28.94, H_2O 1.48, total 100 wt%.

Paratimroseite

The averages (and ranges) of the analyses are: PbO 36.11 (35.28–36.50), CuO 26.27 (26.03–26.73), TeO_3 29.80 (29.62–30.07), Cl 0.04 (0.00–0.10), H_2O 3.01 (structure), O≡Cl –0.01, total 95.22 wt%. The empirical formula (based on O+Cl = 14) is $Pb_{1.94}Cu^{2+}_{3.96}Te^{6+}_{2.03}O_{12}(H_2O)_{1.99}Cl_{0.01}$. The simplified formula is $Pb_2Cu^{2+}_4(Te^{6+}O_6)_2(H_2O)_2$, which requires PbO 38.76, CuO 27.62, TeO_3 30.49, H_2O 3.13, total 100 wt%.

X-ray crystallography and structure determinations

All powder and single-crystal X-ray diffraction data were obtained on a Rigaku R-Axis Spider curved imaging plate microdiffractometer utilizing monochromatized Mo*K*α radiation. The powder data for timroseite and paratimroseite are presented in Table 1. The observed powder data for both minerals fit those calculated from their respective structures well. Figure 5 compares the powder patterns for the two minerals and shows them to be strikingly different in spite of the nearly identical unit cells.

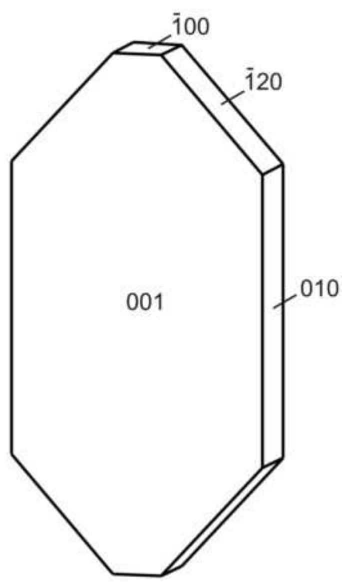

FIGURE 4. Crystal drawing of paratimroseite (clinographic projection).

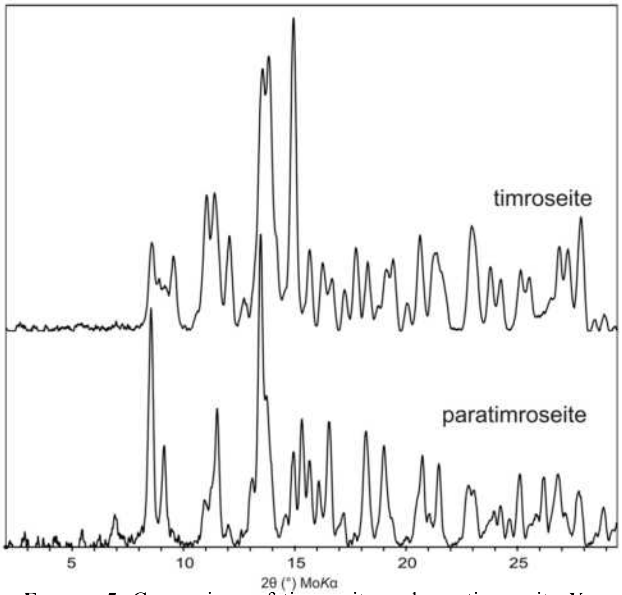

FIGURE 5. Comparison of timroseite and paratimroseite X-ray powder-diffraction patterns.

The Rigaku CrystalClear software package was used for processing the structure data. Numerical (shape-based) and empirical absorption corrections were tested for each data set. The crystal of timroseite used for data collection was a relatively equant (50 × 33 × 25 μm) rhomb of equal dimensions, for which an empirical absorption correction provided the best R_{int} and structure refinement. The crystal of paratimroseite is a very small, thin (45 × 25 × 6 μm) blade, for which a shape-based absorption correction worked best. The structures were solved by direct methods using SIR92 (Altomare et al. 1994) and refined, with neutral atom scattering factors, using SHELXL-97 software (Sheldrick 2008).

The location of all non-hydrogen atoms in the timroseite structure was straightforward and, with anisotropic displacement parameters assigned to all atoms, the structure refined to R_1 = 0.053 for 1181 reflections with $F_o > 4\sigma F$. The Flack parameter (Flack and Bernardinelli 1999), 0.47(2), indicated the likely presence of merohedral twinning. After adding the TWIN instruction, R_1 improved to 0.040; however, two large residuals of 7.0 and 4.9 e/Å^3 remained at 0.89 Å from Pb2 and 0.77 Å from Pb1, respectively. On the presumption that these represented alternate Pb sites, they were refined as such. With the occupancies of

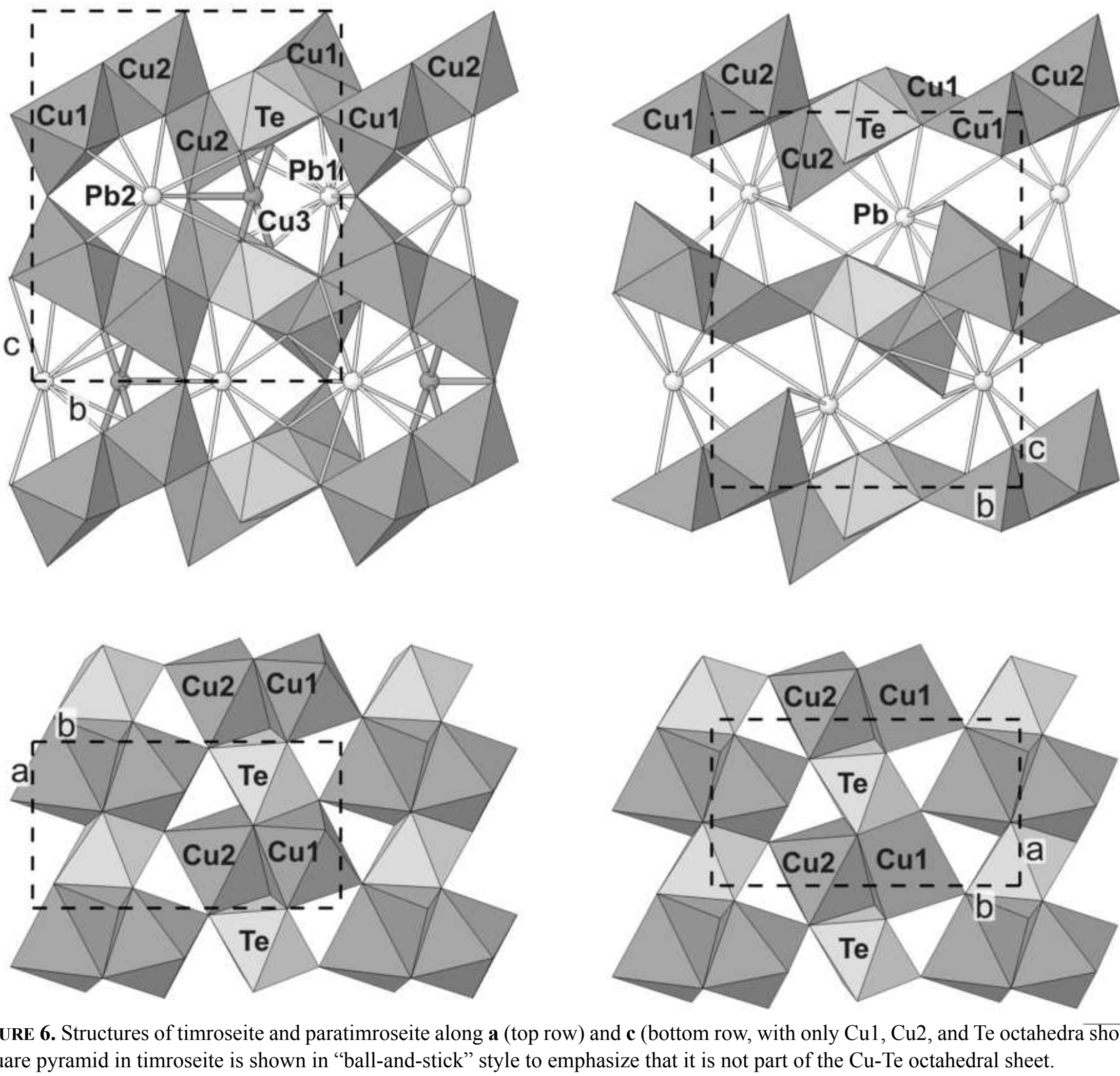

FIGURE 6. Structures of timroseite and paratimroseite along **a** (top row) and **c** (bottom row, with only Cu1, Cu2, and Te octahedra shown). The Cu3 square pyramid in timroseite is shown in "ball-and-stick" style to emphasize that it is not part of the Cu-Te octahedral sheet.

TABLE 1. X-ray powder-diffraction data for timroseite and paratimroseite

timroseite

I_{obs}	d_{obs}	d_{calc}	I_{calc}	*hkl*
27	4.754	4.745	31	101*
15	4.582	4.579	11	110*
13	4.442	4.442	8	021*
23	4.269	4.256	26	111*
43	3.693	3.696	48	022*
44	3.578	3.587	39	112*
		3.534	22	120
30	3.383	3.379	39	121*
10	3.205	3.209	12	030*
		3.093	14	103
		3.014	13	122
84	3.008	3.005	58	023*
88	2.950	2.945	100	113*
30	2.870	2.885	43	004
13	2.813	2.804	16	032
100	2.732	2.731	100	130*
		2.658	7	131
26	2.606	2.603	17	200*
		2.602	14	123
22	2.512	2.513	19	210*
		2.469	6	132
		2.455	8	211
16	2.451	2.441	18	114
13	2.369	2.372	14	202*
		2.356	6	041
27	2.302	2.304	25	212*
		2.246	7	221
22	2.236	2.235	22	124*
		2.227	4	133
8	2.181	2.184	9	140
19	2.139	2.146	9	141
		2.145	7	034
		2.128	12	222
23	2.106	2.103	19	213*
9	2.040	2.040	12	043*
		1.991	6	231
30	1.983	1.983	29	134*
		1.967	7	223
24	1.925	1.932	8	204
		1.932	8	125
		1.923	8	006
19	1.895	1.899	5	143
		1.899	5	051
		1.895	10	214
33	1.785	1.793	10	224
		1.789	8	233
		1.786	10	026
		1.784	8	151
		1.773	22	116
		1.767	5	240
20	1.722	1.723	15	152*
		1.722	3	053
16	1.689	1.690	7	242*
		1.689	7	311*
		1.689	5	126
19	1.630	1.635	9	153
		1.632	4	320
		1.625	8	225
17	1.605	1.606	6	243*
		1.604	6	060*
10	1.550	1.561	5	313
		1.551	6	117
		1.546	5	062
27	1.527	1.533	3	160
		1.531	4	154
		1.527	9	216*
		1.526	8	330*
26	1.506	1.513	3	331
		1.507	17	244*
		1.503	5	323
		1.502	5	046
36	1.475	1.482	5	162
		1.476	20	332*
		1.473	9	226
		1.469	8	314
3	1.443	1.442	4	008
5	1.422	1.422	6	155

paratimroseite

I_{obs}	d_{obs}	d_{calc}	I_{calc}	*hkl*
10	5.887	5.845	10	002
		4.819	12	020
76	4.771	4.759	61	101*
32	4.463	4.455	31	021*
14	3.719	3.718	12	022
18	3.623	3.612	11	013
		3.607	6	112
44	3.544	3.538	36	120*
22	3.122	3.121	16	103*
100	3.029	3.030	54	023*
		3.027	46	122*
48	2.973	2.969	37	113
27	2.916	2.922	19	004
10	2.799	2.797	8	014
30	2.733	2.735	12	130*
41	2.665	2.663	41	131*
		2.619	5	123
27	2.608	2.606	17	200*
21	2.539	2.543	17	201*
		2.477	10	132
40	2.469	2.464	33	114*
6	2.408	2.410	5	040
11	2.378	2.380	7	202
		2.253	9	124
34	2.246	2.249	20	221*
		2.228	12	042
		2.166	8	203
30	2.151	2.150	22	141*
		2.133	5	105
9	2.109	2.113	6	213
14	1.998	1.997	10	134
29	1.975	1.976	23	223*
10	1.944	1.945	6	204
26	1.908	1.907	14	143*
		1.906	8	214
18	1.800	1.803	8	224
		1.793	5	116
		1.787	6	151
17	1.778	1.777	8	135
		1.769	5	240
4	1.750	1.740	3	205
6	1.723	1.728	2	053
		1.727	2	152
8	1.712	1.718	3	301
		1.707	4	126
10	1.692	1.693	8	242
6	1.665	1.666	5	036
		1.664	3	234
20	1.635	1.637	7	225*
		1.634	7	320*
4	1.607	1.611	2	243
		1.606	2	060
7	1.589	1.591	2	061
		1.587	2	136
		1.587	3	303
19	1.568	1.569	15	117*
7	1.548	1.549	5	062
20	1.531	1.537	9	154
		1.535	5	160
		1.530	4	235
		1.528	8	330
8	1.513	1.515	4	046
17	1.482	1.485	5	063
		1.485	5	162
		1.478	6	332
4	1.443	1.445	2	018
13	1.426	1.430	7	155*
		1.426	3	324
		1.425	2	137
		1.423	4	333

TABLE 1.—CONTINUED

I_{obs}	d_{obs}	d_{calc}	I_{calc}	*hkl*
5	1.405	1.411	2	245
		1.404	1	236
		1.399	4	341
10	1.394	1.392	4	118
		1.391	3	217
4	1.375	1.380	3	315
		1.370	2	056
12	1.357	1.358	8	261*
		1.354	3	334
5	1.324	1.325	4	343
17	1.288	1.290	5	263
		1.288	3	237
		1.285	4	316
7	1.269	1.272	5	402
5	1.260	1.263	1	218
		1.260	1	173
8	1.249	1.250	4	421

Notes: I_{obs} based upon peak heights. I_{calc} calculated from the crystal structure using Powder Cell (Kraus and Nolze 1996). d_{calc} based on the cell refined from the powder data (*) using UnitCell (Holland and Redfern 1997). Refined cell for timroseite: $a = 5.2054(5)$, $b = 9.626(1)$, $c = 11.538(2)$ Å, and $V = 578.1(1)$ Å^3. Refined cell for paratimroseite: $a = 5.2109(7)$, $b = 9.638(1)$, $c = 11.689(2)$ Å, and $V = 587.0(1)$ Å^3.

all four Pb sites refined independently, R_1 improved to 0.029. The combined occupancies of each paired site (Pb1 = 0.94 and Pb1a = 0.09; Pb2 = 0.84 and Pb2a = 0.17) is close to 1, clearly supporting the modeling of the residuals as alternate Pb sites. In the final refinement, the Pb1-Pb1a and Pb2-Pb2a distances were 0.40 and 0.54 Å, respectively.

The location of all non-hydrogen atoms in the paratimroseite structure was also straightforward. With anisotropic displacement parameters assigned to all atoms, the structure refined to $R_1 = 0.038$ for 842 reflections with $F_o > 4\sigma F$; however, the anisotropic displacement parameters for two O atoms, O2 and O3, went slightly non-positive definite. In the final refinement, O2 and O3 were assigned isotropic displacement parameters yielding $R_1 = 0.039$. The very small size of the crystal used in the data collection resulted in weak intensities for higher-angle reflections, contributing to the relatively high R_{int} (0.1114) and probably also to the problems in refining the anisotropic displacement parameters for O2 and O3. The Flack parameter, 0.02(2), indicated the lack of merohedral twinning.

Bond-valence calculations for timroseite indicate that two O atoms (designated OH1 and OH2) are hydroxyl groups. Bond-valence calculations for paratimroseite indicate that one O atom (designated OW) is a water molecule; however, the quality of the data did not allow the unambiguous determination of the H atom sites for either structure. Hydrogen bonds were assigned on the basis of bond valence, bond geometry, and bond distance. In timroseite, OH1 is situated 2.87 Å from two O6 atoms along edges of two separate $Cu1O_6$ octahedra. The H atom is probably located between the two O6 atoms, forming a bifurcated hydrogen bond. The OH2 is 3.02 Å from two O6 atoms and probably forms a hydrogen bond to one O6 or the other (or effectively a half bond to each). In paratimroseite, OW forms two likely hydrogen bonds to O1 and O6.

The details of the data collections and the final refinements for both structures are provided in Table 2. The final atomic coordinates and displacement parameters for timroseite are in

TABLE 2. Data collection and structure refinement details for timroseite and parartimroseite

	Timroseite	Paratimroseite
Diffractometer	Rigaku R-Axis Spider	
X-ray radiation/power	MoKα (λ = 0.71075 Å)/50 kV, 40 mA	
Temperature	298(2) K	298(2) K
Structural formula	$Pb_2Cu^{2+}_5(Te^{6+}O_6)_2(OH)_2$	$Pb_2Cu^{2+}_4(Te^{6+}O_6)_2(H_2O)_2$
Space group	$P2_1nm$	$P2_12_12_1$
Unit-cell dimensions	$a = 5.1999(2)$ Å	$a = 5.1943(4)$ Å
	$b = 9.6225(4)$ Å	$b = 9.6198(10)$ Å
	$c = 11.5340(5)$ Å	$c = 11.6745(11)$ Å
Z	2	2
Volume	577.13(4) Å^3	583.35(9) Å^3
Density (for above formula)	6.982 g/cm^3	6.557 g/cm^3
Absorption coefficient	43.137 mm^{-1}	40.901 mm^{-1}
F(000)	1054	1000
Crystal size (μm)	50 × 33 × 25	45 × 25 × 6
θ range	4.12 to 26.36°	3.49 to 24.70°
Index ranges	$-6 \le h \le 6$	$-5 \le h \le 6$
	$-12 \le k \le 12$	$-11 \le k \le 11$
	$-14 \le l \le 14$	$-13 \le l \le 13$
Reflections collected/unique	12601/1227	4431/884
	[$R_{int} = 0.0766$]	[$R_{int} = 0.1114$]
Reflections with $F_o > 4\sigma F$	1181	842
Completeness to max. θ	99.1%	99.8%
Max. and min. transmission	0.4119 and 0.2216	0.7914 and 0.2605
Refinement method	Full-matrix least-squares on F^2	
Parameters refined	128	91
GoF	1.064	0.974
Final R indices [$F_o > 4\sigma F$]	$R_1 = 0.029$,	$R_1 = 0.039$,
	w$R_2 = 0.064$	w$R_2 = 0.073$
R indices (all data)	$R_1 = 0.030$,	$R_1 = 0.050$,
	w$R_2 = 0.064$	w$R_2 = 0.078$
Largest diff. peak / hole	1.930 / –1.372 e/Å^3	1.708 / –2.210 e/Å^3

Notes: $R_{int} = \Sigma|F_o^2 - F_o^2(\text{mean})|/\Sigma[F_o^2]$. GoF = $S = \{\Sigma[w(F_o^2 - F_c^2)^2]/(n-p)\}^{1/2}$. $R_1 = \Sigma||F_o| - |F_c||/\Sigma|F_o|$. $wR_2 = \{\Sigma[w(F_o^2 - F_c^2)^2]/\Sigma[w(F_o^2)^2]\}^{1/2}$. $w = 1/[\sigma^2(F_o^2) + (aP)^2 + bP]$ where P is $[2F_c^2 + \text{Max}(F_o^2,0)]/3$; for timroseite a is 0.0333 and b is 3.4705; for paratimroseite a is 0 and b is 0.

TABLE 3. Atomic coordinates and displacement parameters (Å^2) for timroseite

	x	y	z	U_{eq}	U_{11}	U_{22}	U_{33}	U_{23}	U_{13}	U_{12}
Pb1*	0.1230(4)	0.0356(5)	0.0	0.0229(7)	0.0198(11)	0.0213(13)	0.0277(6)	0	0	0.0041(7)
Pb1a*	0.125(9)	0.077(8)	0.0	0.060(11)	0.11(3)	0.037(19)	0.035(8)	0	0	0.032(13)
Pb2*	0.3820(7)	0.38682(17)	0.5	0.0208(11)	0.0170(17)	0.0178(13)	0.0277(7)	0	0	0.0013(6)
Pb2a*	0.279(13)	0.396(3)	0.5	0.062(7)	0.07(2)	0.075(8)	0.045(5)	0	0	–0.018(8)
Te	0.2005(4)	0.74917(7)	0.24990(7)	0.0122(2)	0.0109(3)	0.0092(4)	0.0165(4)	0.0003(3)	0.0001(3)	–0.0004(2)
Cu1	0.6694(4)	0.89920(14)	0.18488(13)	0.0146(4)	0.0131(9)	0.0093(7)	0.0214(8)	–0.0021(5)	0.0017(6)	0.0003(6)
Cu2	0.7204(4)	0.59878(15)	0.32206(14)	0.0155(4)	0.0136(7)	0.0108(7)	0.0220(9)	–0.0022(6)	0.0036(6)	–0.0026(7)
Cu3	0.1304(7)	0.7144(2)	0.5	0.0222(5)	0.0194(11)	0.0267(11)	0.0204(11)	0	0	0.0026(10)
O1	0.3817(19)	0.6747(8)	0.3817(7)	0.0160(17)	0.006(4)	0.021(4)	0.021(4)	0.001(3)	0.004(4)	0.009(4)
O2	0.0013(18)	0.8259(9)	0.1236(7)	0.0143(17)	0.015(4)	0.014(4)	0.014(4)	0.006(4)	–0.005(4)	–0.005(3)
O3	0.3533(19)	0.9309(7)	0.2788(8)	0.0189(19)	0.021(5)	0.010(4)	0.025(5)	–0.002(3)	–0.005(5)	–0.004(4)
O4	0.9192(17)	0.7716(8)	0.3612(8)	0.0135(18)	0.010(4)	0.014(4)	0.016(4)	0.002(3)	–0.003(4)	–0.006(4)
O5	0.0365(18)	0.5718(8)	0.2178(8)	0.0160(19)	0.011(4)	0.006(4)	0.031(5)	–0.001(4)	0.008(4)	0.005(3)
O6	0.5044(19)	0.7173(9)	0.1587(8)	0.018(2)	0.022(5)	0.005(4)	0.026(5)	–0.009(4)	0.007(4)	–0.005(3)
OH1	0.530(3)	0.9473(14)	0.0	0.021(3)	0.017(6)	0.023(7)	0.023(7)	0	0	0.002(6)
OH2	0.798(3)	0.5066(15)	0.5	0.024(3)	0.010(6)	0.040(8)	0.022(7)	0	0	0.003(6)

* Refined occupancies: Pb1 = 0.94(3), Pb1a = 0.09(3), Pb2 = 0.84(3), Pb2a = 0.17(3).

Table 3 and those for paratimroseite are in Table 4. Selected interatomic distances for both structures are listed and compared in Table 5 and bond valences in Table 6. CIF and structure factors available on deposit[1].

Description of the structures

The unit-cell dimensions for timroseite and paratimroseite are so similar that based solely on those dimensions and the qualitative chemistry one might readily conclude that the two minerals are identical; however, the powder-diffraction data clearly show the minerals to be different, as do the space groups and quantitative chemical analyses. Not surprisingly, the crystal structures of the two minerals are very closely related (Fig. 6).

Both structures are based upon edge- and corner-sharing linkages of $Te^{6+}O_6$ and $Cu^{2+}O_6$ octahedra and $Cu^{2+}O_5$ square pyramids, with Pb atoms occupying the space between and forming further linkages via Pb-O bonds. The TeO_6 octahedra are reasonably regular in both structures with Te-O distances from 1.924 to 1.958 Å in timroseite and from 1.892 to 1.959 Å in paratimroseite and angles from 83.6 to 96.7° in timroseite and from 82.4 to 98.3° in paratimroseite. The Cu polyhedra exhibit typical Jahn-Teller 4+2 and 4+1 distortions with four short equatorial Cu-O bonds and one or two long apical Cu-O bonds (Table 4).

In timroseite, the Pb1 and Pb2 sites are 12- and 11-fold coordinated, respectively. The alternate Pb sites, Pb1a and Pb2a, are coordinated by the same O atoms and most likely reflect a shifting of the Pb atoms within their coordination spheres (see Table 5 and Fig. 7). For the bond-valence analysis in Table 6, Pb1 and Pb2 sites are considered fully occupied and the Pb1a and Pb2a sites are ignored; however, it is worth noting that the Pb1a and Pb2a sites receive bond-valence sums of 1.80 and 1.88, as compared to 1.98 and 2.04 for the the Pb1 and Pb2 sites. In paratimroseite, the Pb atom is 12-fold coordinated (see Table 5 and Fig. 7). All of the Pb coordinations in timroseite and paratimroseite are lopsided as is typical for Pb^{2+} with stereoactive $6s^2$ lone electron pairs (e.g., Moore 1988; Cooper and Hawthorne 1994; Kharisun et al. 1997; Mills et al. 2009a). In fact, the Pb atoms in the structures of all seven recently discovered new minerals from Otto Mountain exhibit this feature.

The Te, Cu1, and Cu2 polyhedra in the two structures form edge- and corner-sharing sheets parallel to (001) and these sheets are identical in topology and virtually identical in geometry. The only significant difference between the sheets is that in timroseite Cu1 is in sixfold coordination and in paratimroseite Cu1 is in fivefold coordination. This difference also relates to the linkage between the sheets in the two structures. Successive sheets in

[1] Deposit item AM-10-047, CIF and structure factors. Deposit items are available two ways: For a paper copy contact the Business Office of the Mineralogical Society of America (see inside front cover of recent issue) for price information. For an electronic copy visit the MSA web site at http://www.minsocam.org, go to the *American Mineralogist* Contents, find the table of contents for the specific volume/issue wanted, and then click on the deposit link there.

Table 5. Selected bond distances (Å) for timroseite and paratimroseite

Timroseite			Paratimroseite	
Pb1-OH1	2.280(14)	2.45(5)*	Pb-O2	2.348(13)
Pb1-O2(×2)	2.550(9)	2.88(7)	Pb-O6	2.419(14)
Pb1-O4(×2)	2.894(10)	2.65(7)	Pb-O5	2.546(13)
Pb1-O3(×2)	2.929(9)	2.92(2)	Pb-OW	2.714(17)
Pb1-OH1	3.199(14)	3.34(6)	Pb-O4	2.737(15)
Pb1-O1(×2)	3.347(9)	3.03(6)	Pb-O3	2.962(13)
Pb1-O3(×2)	3.577(9)	3.71(3)	Pb-O1	3.055(15)
<Pb1-O>	3.006	3.01	Pb-OW	3.090(17)
			Pb-O5	3.124(14)
Pb2-OH2	2.452(15)	2.90(6)*	Pb-O4	3.578(15)
Pb2-O2(×2)	2.571(9)	2.81(5)	Pb-O6	3.662(15)
Pb2-O5(×2)	2.668(10)	2.86(3)	Pb-O1	3.799(13)
Pb2-O6(×2)	2.865(10)	2.56(3)	<Pb-O>	3.003
Pb2-O1(×2)	3.088(8)	3.06(2)		
Pb2-OH2	3.247(14)	2.72(7)		
Pb2-OH1	3.700(14)	3.55(2)		
<Pb2-O>	2.889	2.89		
Te-O6	1.924(10)		Te-O5	1.892(13)
Te-O1	1.927(9)		Te-O2	1.920(13)
Te-O2	1.934(8)		Te-O4	1.920(13)
Te-O5	1.943(9)		Te-O1	1.929(14)
Te-O3	1.949(8)		Te-O3	1.932(13)
Te-O4	1.958(9)		Te-O6	1.959(13)
<Te-O>	1.938		<Te-O>	1.925
Cu1-O3	1.940(8)		Cu1-O3	1.919(14)
Cu1-O6	1.972(8)		Cu1-O2	1.967(14)
Cu1-O3	1.992(10)		Cu1-O3	1.995(14)
Cu1-O2	1.994(10)		Cu1-O6	2.000(15)
Cu1-OH1	2.300(5)		Cu1-O1	2.423(15)
Cu1-O4	2.707(8)			
<Cu1-O$_{eq}$>	1.975		<Cu1-O$_{eq}$>	1.970
<Cu1-O$_{ap}$>	2.504		<Cu1-O$_{ap}$>	2.423
Cu2-O5	1.954(8)		Cu2-O4	1.999(14)
Cu2-O4	2.010(8)		Cu2-O1	2.001(15)
Cu2-O1	2.027(9)		Cu2-O5	2.018(13)
Cu2-O5	2.053(9)		Cu2-O4	2.034(14)
Cu2-OH2	2.272(6)		Cu2-OW	2.418(13)
Cu2-O6	2.473(10)		Cu2-O2	2.539(13)
<Cu2-O$_{eq}$>	2.011		<Cu2-O$_{eq}$>	2.013
<Cu2-O$_{ap}$>	2.373		<Cu2-O$_{ap}$>	2.479
Cu3-O1(×2)	1.927(9)			
Cu3-O4(×2)	2.019(9)			
Cu3-OH2	2.643(15)			
<Cu3-O$_{eq}$>	1.973			
<Cu3-O$_{ap}$>	2.643			
Hydrogen bonds				
OH1-O6	2.875(14)		OW-O6	2.692(19)
OH2-O6	3.024 (13)		OW-O1	2.693(19)

* Second listed Pb-O distances for timroseite correspond to Pb1a and Pb2a sites.

Table 4. Atomic coordinates and displacement parameters (Å^2) for paratimroseite

	x	*y*	*z*	U_{eq}	U_{11}	U_{22}	U_{33}	U_{23}	U_{13}	U_{12}
Pb	0.48658(16)	0.37646(9)	0.71849(6)	0.0199(2)	0.0182(4)	0.0224(5)	0.0192(4)	0.0041(4)	0.0004(4)	0.0012(5)
Te	0.8986(2)	0.49499(15)	0.49034(11)	0.0124(3)	0.0100(6)	0.0117(7)	0.0155(7)	−0.0003(6)	−0.0003(5)	0.0000(6)
Cu1	0.3802(4)	0.6442(3)	0.5457(2)	0.0148(6)	0.0090(12)	0.0157(15)	0.0196(14)	0.0012(11)	−0.0011(9)	0.0007(12)
Cu2	0.4205(4)	0.3513(3)	0.4222(2)	0.0145(6)	0.0090(13)	0.0159(15)	0.0184(14)	0.0005(11)	−0.0015(10)	−0.0012(11)
O1	0.608(3)	0.5291(15)	0.3914(11)	0.016(3)	0.018(8)	0.015(8)	0.016(8)	0.002(6)	−0.012(6)	−0.007(7)
O2	0.195(3)	0.4730(15)	0.5870(11)	0.012(3)						
O3	0.544(3)	0.8222(14)	0.5322(11)	0.023(4)						
O4	0.741(3)	0.3179(14)	0.5188(12)	0.022(4)	0.018(8)	0.007(8)	0.041(10)	0.005(7)	0.003(7)	−0.010(6)
O5	0.415(3)	0.5715(15)	0.8624(11)	0.017(4)	0.007(8)	0.032(10)	0.012(8)	−0.003(6)	0.000(5)	0.000(7)
O6	0.696(3)	0.5660(16)	0.6193(11)	0.019(4)	0.018(8)	0.028(10)	0.011(8)	−0.002(6)	0.010(6)	0.001(7)
OW	0.473(3)	0.7477(14)	0.2604(10)	0.024(4)	0.043(10)	0.008(8)	0.020(8)	−0.005(6)	0.008(7)	−0.003(8)

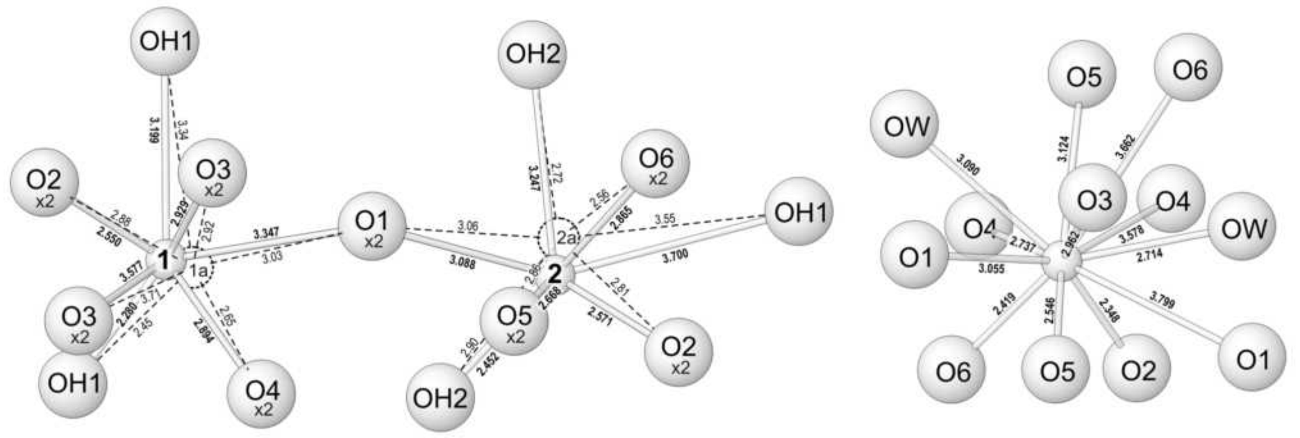

FIGURE 7. Coordinations of Pb atoms in timroseite (left) and paratimroseite (right). For timroseite, the Pb sites (1, 1a, 2, and 2a) and the OH sites are situated on a 001 mirror plane; other O sites are above and below the mirror. Bond lengths are given in angstroms.

TABLE 6. Bond-valence analyses for timroseite (top) and paratimroseite (bottom); values are expressed in valence units

	O1	O2	O3	O4	O5	O6	OH1	OH2	Sum
Te	0.973	0.955	0.917	0.895	0.932	1.003			5.675
Cu1		0.427	0.494, 0.429	0.062		0.453	0.187 ×2↓		2.052
Cu2	0.390			0.409	0.476, 0.364	0.117		0.201 ×2↓	1.957
Cu3	0.512 ×2→			0.399 ×2→				0.074	1.896
Pb1	0.059 ×2→	0.302 ×2→	0.139 ×2→	0.150 ×2→			0.524, 0.080		1.978
			0.037 ×2→						
Pb2	0.101 ×2→	0.289 ×2→			0.237 ×2→	0.159 ×2→	0.029	0.369, 0.073	2.042
H1						0.160 ×½↓	0.840		1.000
H2						0.126 ×½↓		0.874	1.000
Sum	2.035	1.973	2.016	1.915	2.009	1.874	1.847	1.792	

	O1	O2	O3	O4	O5	O6	OW	Sum
Te	0.968	0.992	0.960	0.992	1.070	0.893		5.875
Cu1	0.134	0.459	0.523, 0.426			0.420		1.962
Pb	0.108, 0.024	0.456	0.130	0.206, 0.037	0.304, 0.094	0.394, 0.031	0.216, 0.100	2.100
H1						0.231	0.769	1.000
H2	0.230						0.770	1.000
Sum	1.883	2.005	2.039	2.039	1.868	1.969	1.991	

Notes: Multiplicity is indicated by ×→↓; Pb^{2+}-O bond strengths from Krivovichev and Brown (2001); Cu^{2+}-O and Te^{6+}-O bond strengths from Brown and Altermatt (1985); hydrogen-bond strengths based on O-O distances from Ferraris and Ivaldi (1988); for timroseite, calculations are based on fully occupied Pb sites and satellite Pb sites are not considered.

timroseite are positioned such that peripheral apical O atoms (OH1) of the Cu1 octahedra in adjacent sheets are shared, as are peripheral apical O atoms (OH2) of the Cu2 octahedra. In timroseite, an additional Cu atom (Cu3) with square pyramidal coordination also participates in the inter-sheet linkage by sharing its apical O atom with two Cu2 atoms in different sheets and sharing *trans* equatorial edges with two Te octahedra in different sheets. The addition of the Cu3 square pyramid thereby links the sheets into a framework.

In paratimroseite, the edge- and corner-sharing sheets of Te, Cu1, and Cu2 polyhedra parallel to (001) are shifted such that the peripheral apical O atoms (OW) of the Cu2 octahedra in successive sheets are no longer shared and the Cu1 polyhedron no longer has a peripheral apical O atom, resulting in its square pyramidal coordination. The shifting of the sheets also destroys the local bonding environment required for incorporation of the additional Cu atom (Cu3) in the structure. The sheets in paratimroseite are joined only via Pb-O and H bonds, thus accounting for the good {001} cleavage, which is not observed in timroseite. The lack of strong polyhedral linkages between the sheets in paratimroseite makes it more surprising that its *c* cell dimension is so similar to that of timroseite.

The minerals most closely allied chemically with timroseite and paratimroseite are housleyite, $Pb_6Cu^{2+}Te_4^{6+}O_{18}(OH)_2$ (Kampf et al. 2010c), and khinite (khinite-4*O* and khinite-3*T*), $PbCu_3^{2+}Te^{6+}O_6(OH)_2$ (Burns et al. 1995; Cooper et al. 2008; Hawthorne et al. 2009), and all occur in close association at Otto Mountain. The structures of the khinite polytypes are also based upon edge- and corner-sharing sheets of Te and Cu octahedra; however, the sheets in khinite are very different topologically (and geometrically) from those in timroseite and paratimroseite. The structure of housleyite is completely different in that it possesses corner-sharing chains of TeO_6 octahedra.

ACKNOWLEDGMENTS

We thank Associate Editor Ian Swainson, Technical Editor Ronald C. Petersen, and referees Mark A. Cooper and Andrew C. Roberts for helpful comments on the manuscript. Timothy P. Rose provided for study two of the three cotype specimens of timroseite, from which were obtained the only crystals suitable for single-crystal work. The EMP analyses were supported by a grant to the California Institute of Technology from the Northern California Mineralogical Association. The remainder of this study was funded by the John Jago Trelawney Endowment to the Mineral Sciences Department of the Natural History Museum of Los Angeles County.

References cited

Altomare, A., Cascarano, G., Giacovazzo, C., Guagliardi, A., Burla, M.C., Polidori, G., and Camalli, M. (1994) SIR92—A program for automatic solution of crystal structures by direct methods. Journal of Applied Crystallography 27, 435.

Brown, I.D. and Altermatt, D. (1985) Bond-valence parameters from a systematic analysis of the inorganic crystal structure database. Acta Crystallographica, B41, 244–247.

Burns, P.C., Cooper, M.A., and Hawthorne, F.C. (1995) Parakhinite, $Pb^{2+}Cu_3^{2+}Te^{6+}O_6(OH)_2$: crystal structure and revision of the chemical formula. Canadian Mineralogist, 33, 33–40.

Cooper, M. and Hawthorne, F.C. (1994) The crystal structure of wherryite, $Pb_7Cu_2(SO_4)_4(SiO_4)_2(OH)_2$, a mixed sulfate-silicate with $[^{[6]}M(TO_4)_2\Phi]$ chains. Canadian Mineralogist, 32, 373–380.

Cooper, M.A., Hawthorne, F.C., and Back, M.E. (2008) The crystal structure of khinite and polytypism in khinite and parakhinite. Mineralogical Magazine, 72, 763–770.

Ferraris, G. and Ivaldi, G. (1988) Bond valence vs. bond length in O…O hydrogen bonds. Acta Crystallographica, B44, 341–344.

Flack, H.D. and Bernardinelli, G. (1999) Absolute structure and absolute configuration. Acta Crystallographica, A55, 908–915.

Grundler, P., Brugger, J., Meisser, N., Ansermet, S., Borg, S., Etschmann, B., Testemale, D., and Bolin, T. (2008) Xocolatlite, $Ca_2Mn_2^{4+}Te_2O_{12}\cdot H_2O$, a new tellurate related to kuranakhite: Description and measurement of Te oxidation state by XANES spectroscopy. American Mineralogist, 93, 1911–1920.

Hawthorne, F.C., Cooper, M.A., and Back, M.E. (2009) Khinite-4*O* [= khinite] and khinite-3*T* [= parakhinite]. Canadian Mineralogist, 47, 473–476.

Holland, T.J.B. and Redfern, S.A.T. (1997) Unit cell refinement from powder diffraction data: the use of regression diagnostics. Mineralogical Magazine, 61, 65–77.

Kampf, A.R., Housley, R.M., and Marty, J. (2010a) Lead-tellurium oxysalts from Otto Mountain near Baker, California: III. Thorneite, $Pb_6(Te_2^{6+}O_{10})(CO_3)Cl_2(H_2O)$, the first mineral with edge-sharing tellurate dimers. American Mineralogist, 95, 1548–1553.

Kampf, A.R., Housley, R.M., Mills, S.J., Marty, J., and Thorne, B. (2010b) Lead-tellurium oxysalts from Otto Mountain near Baker, California: I. Ottoite, Pb_2TeO_5, a new mineral with chains of tellurate octahedra. American Mineralogist, 95, 1329–1336.

Kampf, A.R., Marty, J., and Thorne, B. (2010c) Lead-tellurium oxysalts from Otto Mountain near Baker, California: II. Housleyite, $Pb_6CuTe_4O_{18}(OH)_2$, a new mineral with Cu-Te octahedral sheets. American Mineralogist, 95, 1337–1343.

Kampf, A.R., Mills, S.J., Housley, R.M., Marty, J., and Thorne, B. (2010d) Lead-tellurium oxysalts from Otto Mountain near Baker, California: IV. Markcooperite, $Pb_2(UO_2)Te^{6+}O_6$, the first natural uranyl tellurate. American Mineralogist, 95, 1554–1559.

——— (2010e) Lead-tellurium oxysalts from Otto Mountain near Baker, California: VI. Telluroperite, $Pb_3Te^{4+}O_4Cl_2$, the Te analog of perite and nadorite. American Mineralogist, 95, 1569–1573.

Kharisun, Taylor, M.R., Bevan, D.J.M., Rae, A.D., and Pring, A. (1997) The crystal structure of mawbyite, $PbFe_2(AsO_4)_2(OH)_2$. Mineralogical Magazine, 61, 685–691.

Kraus, W. and Nolze, G. (1996) POWDER CELL—a program for the representation and manipulation of crystal structures and calculation of the resulting X-ray powder patterns. Journal of Applied Crystallography, 29, 301–303.

Krivovichev, S.V. and Brown, I.D. (2001) Are the compressive effects of encapsulation an artifact of the bond valence parameters? Zeitschrift für Kristallographie, 216, 245–247.

Mandarino, J.A. (1981) The Gladstone-Dale relationship. IV. The compatibility concept and its application. Canadian Mineralogist, 19, 441–450.

Mills, S.J., Groat, L.A., and Kolitsch, U. (2008) Te, Sb, and W mineralization at the Black Pine mine, Montana. Poster, 18th Annual V.M. Goldschmidt Conference, Vancouver, Canada, July 13–18, 2008. Abstract in Geochimica et Cosmochimica Acta, 72, Special Supplement 12S, A632.

Mills, S.J., Kampf, A.R., Raudsepp, M., and Christy, A.G. (2009a) The crystal structure of Ga-rich plumbogummite from Tsumeb, Namibia, Mineralogical Magazine, 73, 837–845.

Mills, S.J., Kolitsch, U., Miyawaki, R., Groat, L.A., and Poirier, G. (2009b) Joëlbruggerite, $Pb_3Zn_3(Sb^{5+},Te^{6+})As_2O_{13}(OH,O)$, the Sb^{5+} analog of dugganite, from the Black Pine mine, Montana. American Mineralogist, 94, 1012–1017.

Mills, S.J., Kampf, A.R., Kolitsch, U., Housley, R.M., and Raudsepp, M. (2010) The crystal chemistry and crystal structure of kuksite, $Pb_3Zn_3Te^{6+}P_2O_{14}$, and a note on the crystal structure of yafsoanite, $(Ca,Pb)_3Zn(TeO_6)_2$. American Mineralogist, 95, 933–938.

Moore, P.B. (1988) The joesmithite enigma: Note on the $6s^2$ Pb^{2+} lone pair. American Mineralogist, 73, 843–844.

Sheldrick, G.M. (2008) A short history of SHELX. Acta Crystallographica, A64, 112–122.

Manuscript received January 28, 2010
Manuscript accepted May 6, 2010
Manuscript handled by Ian Swainson